# Triplet superconductivity vs. easy-plane ferromagnetism in a 1D itinerant electron system with transverse spin anisotropy

C. Dziurzik, G.I. Japaridze[a], A. Schadschneider[b], and J. Zittartz

Institut für Theoretische Physik, Universität zu Köln, 50937 Köln, Germany

**Abstract.** In this paper we study the ground state phase diagram of a one-dimensional $t - U - J$ model, at half-filling. In the large-bandwidth limit and for ferromagnetic exchange with easy-plane anisotropy, a phase with gapless charge and massive spin excitations, characterized by the coexistence of triplet superconducting and spin density wave instabilities is realized in the ground state. With reduction of the bandwidth, a transition into an insulating phase showing properties of the spin-$\frac{1}{2}$ $XY$ model takes place.

**PACS.** 71.10.Hf Non-Fermi-liquid ground states, electron phase diagrams and phase transitions in model systems – 71.10.Fd Lattice fermion models (Hubbard model, etc.) – 74.20.Mn Nonconventional mechanisms (spin fluctuations, polarons and bipolarons, resonating valence bond model, anyon mechanism, marginal Fermi liquid, Luttinger liquid, etc.) – 71.27.+a Strongly correlated electron systems; heavy fermions – 75.10.Pq Spin chain models

## 1 Introduction

Superconductivity near a magnetic instability is a topic of increased current interest in condensed matter physics. Magnetically mediated Cooper pairing near the antiferromagnetic instability is widely discussed in the context of superconductivity in copper-oxide systems [1]. Moreover, the discovery of Triplet Superconductivity (TS) in $Sr_2RuO_4$ [2] and the recent discovery of coexistence of the TS phase with ferromagnetism in $UGe_2$ [3], URhGe [4] and $ZrZn_2$ [5] has triggered an increased activity in studies of correlated electron models showing close proximity of triplet superconducting and ferromagnetically ordered phases [6–14].

Another group of unconventional superconductors with close proximity of magnetic and superconducting ordering belongs to the $(TMTSF)_2X$ family of quasi-one-dimensional conductors (Bechgaard salts) [15,16]. Growing experimental evidence has been collected in the last few years, indicating that $(TMTSF)_2ClO_4$ and $(TMTSF)_2PF_6$ under pressure are triplet superconductors [17]. Most interesting is the phase diagram of $(TMTSF)_2PF_6$ which shows a spin-Peierls (SP) phase in the ground state at atmospheric pressure. Increasing pressure leads first to a transition from the SP phase into a spin density wave (SDW) phase, and finally to the suppression of the SDW ground state in favor of supercon-

ductivity [18]. Recent detailed experimental studies of the phase diagram of the $(TMTSF)_2PF_6$ compound indicate the possibility of a *coexistence regime* between SDW and superconductivity [19]. Although the very presence of a *homogeneous* coexistence phase in the phase diagram was questioned in the more recent publication [20], the SDW-SC competition is common in organic materials [21] and therefore models of correlated electrons exhibiting such phases are of great interest.

Various models of strongly correlated electrons showing close proximity of magnetic (ferromagnetic) and superconducting (triplet superconducting) phases have been subject of intensive research in attempt to construct a theoretical model for new superconducting materials. Usually these models are based on some extensions of the Hubbard model. In particular, several extended versions of the repulsive Hubbard model have been employed for a long time as standard models for metal-insulator transitions, antiferromagnetism and high-$T_c$ superconductivity [22]. At the same time, the Hubbard model in the case of sufficiently narrow band and/or low doping is a standard model for metallic ferromagnetism of itinerant electrons [23].

Taking into account the experimentally observed easy-plane anisotropy of the spin exchange [24] in some of these materials, Japaridze and Müller-Hartmann [25] proposed a rather simple extension of the Hubbard model with transverse ($XY$-type) anisotropy as a suitable approach to such systems with coexisting orders. Indeed, this model was shown to exhibit an extremely rich

[a] *Permanent address:* Andronikashvili Institute of Physics, Georgian Academy, Tamarashvili 6, Tbilisi 380077, Georgia
[b] e-mail: `as@thp.uni-koeln.de`

*weak-coupling* phase diagram. In particular in the case of a half-filled band the weak-coupling ground state phase diagram consists of two insulating antiferromagnetic phases with easy-plane anisotropy and a spin gapful metallic phase with an identical decay of the *triplet superconducting* and spin density wave ($SDW^{(z)}$) instabilities. Strong evidence for the presence of an additional transition into a *ferromagnetic XY* phase has also been given [25].

The model describes a system of itinerant electrons with transverse spin-exchange interaction between electrons on nearest-neighbor sites. The one-dimensional version of the Hamiltonian reads:

$$\mathcal{H} = -t \sum_{n,\alpha} \left( c_{n,\alpha}^\dagger c_{n+1,\alpha} + c_{n+1,\alpha}^\dagger c_{n,\alpha} \right)$$
$$+ U \sum_n \rho_\uparrow(n) \rho_\downarrow(n) + \frac{J_{xy}}{2} \sum_n \left( S_n^+ S_{n+1}^- + \text{h.c.} \right). \quad (1)$$

Here $c_{n,\alpha}^\dagger$ ($c_{n,\alpha}$) is the creation (annihilation) operator for an electron at site $n$ with spin $\alpha$, $\rho_{,\alpha}(n) = c_{n,\alpha}^\dagger c_{n,\alpha}$, $\mathbf{S}(n) = \frac{1}{2} c_{n,\alpha}^\dagger \sigma_{\alpha\beta} c_{n,\beta}$ where $\sigma^i$ ($i = x, y, z$) are the Pauli matrices. Below we restrict our consideration to the case of repulsive on-site interaction $U \geq 0$ while the sign of the exchange interaction is arbitrary.

One can easily verify that besides the obvious U(1) spin symmetry in the half-filled case the model is characterized by a SU(2) charge symmetry. An electron-hole transformation for one spin component interchanges the charge and spin degrees of freedom, and maps (1) to the attractive Hubbard model with pair-hopping interaction [26,27].

That the TS phase can be realized in 1D correlated electron systems is well known from standard "*g-ology*" studies [28]. The extended ($U$-$V$) Hubbard model with nearest-neighbor attraction ($V < 0$) has been intensively studied to explain the competition between SDW and superconducting instabilities in TMTSF compounds [29]. However, due to spin rotational invariance, in the extended Hubbard model the TS phase is realized only in the Luttinger liquid phase for $|U| < -2V$ [28,30,31], where both charge and spin excitations are gapless. Singlet superconducting (SS) and TS correlations show identical power-law decay at large distances and the TS instability dominates only due to weak logarithmic corrections [31]. On the other hand, in the spin gapped phase $U < 2V$, the dynamical generation of a spin gap leads to the *complete suppression* of the TS and SDW instabilities. In marked contrast, the ferromagnetic transverse exchange between electrons on neighboring sites provides the possibility for realization of the SDW-TS phase in the case of gapped spin excitation spectrum [25].

In this paper we study the model (1) in the case of a half-filled band using the DMRG techniques. We investigate the excitation spectrum of the system as well as the behavior of various correlation functions. Our numerical results confirm the predictions of a weak-coupling analysis. In addition, we study in detail the strong-coupling sector of the phase diagram, focusing our attention on the

ferromagnetic transition. With increasing transverse ferromagnetic exchange this will reveal the possibility for *two different* scenarios of transition into the easy-plane $XY$ ferromagnetic phase: in the case of weak on-site repulsion ($U < U_c \simeq 2t$) the first transition at $J_{xy} = J_{xy}^{(c1)}$ takes place from a spin gapped metallic phase into the insulating $SDW^{(z)}$ phase with long-range order (LRO) and the latter becomes unstable towards the spin-flop transition into the *ferromagnetic XY* phase at $J_{xy}^{(c2)}$. On the other hand, in the case of strong on-site repulsion, the metallic phase is absent and only the spin-flop transition from the $SDW^{(z)}$ phase into the *ferromagnetic XY* phase takes place at $J_{xy}^{(c2)}$. The critical value of the exchange strongly depends on the on-site repulsion. At $U = 0$, $J_{xy}^{(c1)} = -3t$ and $J_{xy}^{(c2)} = -4t$. In the case of weak $U \ll t$ these parameters are renormalized linearly in $U$, $J_{xy}^{(c1)} = 0$ at $U \simeq 2t$, while for $U \gg t$ we have $J_{xy}^{(c2)} \sim 1/U$.

The paper is organized as follows: in the next section the weak-coupling continuum-limit version of the model is investigated. In Section 3 results of DMRG studies for chains up to $L = 120$ sites are presented. Finally, Section 4 is devoted to a discussion and concluding remarks.

## 2 The continuum-limit theory

In this section we consider the low-energy effective field theory of the initial lattice model. Although this procedure has a long history and is reviewed in many places [32], for clarity we briefly sketch the most important points and fix our notation and conventions. Considering the weak-coupling limit, $|U|, |J_{xy}| \ll t$ we linearize the spectrum and pass to the continuum limit by substituting

$$c_{n,\alpha} \to i^n R_\alpha(x) + (-i)^n L_\alpha(x) \quad (2)$$

$x = na_0$, where $a_0$ is the lattice spacing, and $R_\alpha(x)$ and $L_\alpha(x)$ describe the R(*ight*) and L(*eft*) excitations with dispersion relations $E = \pm v_F p$. These fields are assumed to be smooth on the scale of the lattice spacing and can be bosonized in a standard way [32]

$$R_\alpha(x) = \frac{1}{\sqrt{2\pi a_0}} e^{i\sqrt{4\pi}\Phi_{R,\alpha}}(x), \quad (3)$$

$$L_\alpha(x) = \frac{1}{\sqrt{2\pi a_0}} e^{-i\sqrt{4\pi}\Phi_{L,\alpha}}(x) \quad (4)$$

where $\Phi_{R(L),\alpha}(x)$ are the Right (Left) moving Bose fields, carrying spin $\alpha$. Next we define

$$\phi_\alpha = \phi_{L,\alpha} + \phi_{R,\alpha}, \qquad \theta_\alpha = \phi_{L,\alpha} - \phi_{R,\alpha} \quad (5)$$

and introduce linear combination

$$\varphi_c = (\phi_\uparrow + \phi_\downarrow)/\sqrt{2}, \qquad \vartheta_c = (\theta_\uparrow + \theta_\downarrow)/\sqrt{2}, \quad (6)$$

$$\varphi_s = (\phi_\uparrow - \phi_\downarrow)/\sqrt{2}, \qquad \vartheta_s = (\theta_\uparrow - \theta_\downarrow)/\sqrt{2} \quad (7)$$

to describe the *charge* ($c$) and *spin* ($s$) degrees of freedom, respectively. Then the Hamiltonian density of the

bosonized model is given by

$$\mathcal{H} = \mathcal{H}_c + \mathcal{H}_s,$$

$$\mathcal{H}_c = v_c \int dx \left\{ \frac{1}{2} [(\partial_x \varphi_c)^2 + (\partial_x \vartheta_c)^2] \right.$$

$$\left. + \frac{M_c^0}{a_0^2} \cos \left( \sqrt{8\pi K_c^0} \varphi_c \right) \right\}, \tag{8}$$

$$\mathcal{H}_s = v_s \int dx \left\{ \frac{1}{2} \left[ (\partial_x \vartheta_s)^2 + (\partial_x \varphi_s)^2 \right] \right.$$

$$\left. + \frac{M_s^0}{a_0^2} \cos \left( \sqrt{8\pi K_s^0} \varphi_s \right) \right\}. \tag{9}$$

Here we have defined

$$2 \left( K_c^0 - 1 \right) = g_c = -\frac{1}{\pi \tilde{v}_F} \left( U + J_{xy} \right), \tag{10}$$

$$2\pi M_c^0 = g_u = -\frac{1}{\pi \tilde{v}_F} \left( U + J_{xy} \right), \tag{11}$$

$$2 \left( K_s^0 - 1 \right) = g_s = \frac{1}{\pi \tilde{v}_F} \left( U + J_{xy} \right), \tag{12}$$

$$2\pi M_s^0 = g_\perp = \frac{1}{\pi \tilde{v}_F} \left( U - J_{xy} \right), \tag{13}$$

$$v_{c(s)} = \frac{\tilde{v}_F}{K_{c(s)}^0}, \qquad \tilde{v}_F = 2t \left( 1 + \frac{J_{xy}}{2\pi t} \right). \tag{14}$$

This mapping of the lattice electron system model onto the quantum theory of two independent quantum Bose fields described in terms of an "effective" sine-Gordon (SG) Hamiltonians (8) and (9) will allow to extract the ground state properties of the initial model using the far-infrared properties of the quantum SG theory.

The infrared behavior of the SG Hamiltonian is described by the corresponding pair of renormalization group (RG) equations for the effective coupling constants $K_{c(s)}(l)$ and $M_{c(s)}(l)$

$$\frac{dM_{c(s)}(l)}{dl} = -2 \left( K_{c(s)}(l) - 1 \right) M_{c(s)}(l)$$

$$\frac{dK_{c(s)}(l)}{dl} = -\frac{1}{2} M_{c(s)}^2(l) \tag{15}$$

where $l = \ln(a_0)$ and the bare values of the coupling constants are $K_{c(s)}(l = 0) \equiv K_{c(s)}^0$ and $M_{c(s)}(l = 0) \equiv M_{c(s)}^0$. The pair of RG equations (15) describes the Kosterlitz-Thouless transition [33].

The flow lines lie on the hyperbola

$$4 \left( K_{c(s)} - 1 \right)^2 - M_{c(s)}^2 = \mu^2 = 4(K_{c(s)}^0 - 1)^2 - (M_{c(s)}^0)^2 \tag{16}$$

and exhibit two different regimes depending on the relation between the bare coupling constants [34].

*Weak-coupling regime.* For $2(K_{c(s)} - 1) \geq \left| M_{c(s)}^0 \right|$ we are in the weak-coupling regime: the effective mass $\mathcal{M}_{c(s)} \to 0$. The low energy (large distance) behavior of the corresponding gapless mode is described by a free scalar field.

The vacuum averages of exponentials of the corresponding fields show a power-law decay at large distances ($\eta \equiv c, s$)

$$\left\langle e^{i\sqrt{2\pi K_\eta} \varphi_\eta(x)} e^{-i\sqrt{2\pi K_\eta} \varphi_\eta(x')} \right\rangle \sim |x - x'|^{-K_\eta}, \tag{17}$$

$$\left\langle e^{i\sqrt{2\pi / K_\eta} \vartheta_\eta(x)} e^{-i\sqrt{2\pi / K_\eta} \vartheta_\eta(x')} \right\rangle \sim |x - x'|^{-1/K_\eta}, \tag{18}$$

and the only parameter controlling the infrared behavior in the gapless regime is the fixed-point value of the effective coupling constants $K_{c(s)}^* = K_{c(s)}(l = \infty)$ determined from the equation (16). Note that in the SU(2) symmetric case $\mu = 0$ and $K_{c(s)}^* = 1$.

*Strong coupling regime.* For $2(K_{c(s)}^0 - 1) < \left| M_{c(s)}^0 \right|$ the system scales to strong coupling: depending on the sign of the bare mass $M_{c(s)}^0$, the renormalized mass $\mathcal{M}_{c(s)}$ is driven to $\pm\infty$, signaling a crossover to one of two strong coupling regimes with a dynamical generation of a commensurability gap in the excitation spectrum. The flow of $\left| \mathcal{M}_{c(s)} \right|$ to large values indicates that the $\mathcal{M}_{c(s)} \cos \sqrt{8\pi K} \phi$ term in the sine-Gordon model dominates the long-distance properties of the system. Depending on the sign of the mass term, the field $\varphi$ gets ordered with the expectation values [35]

$$\langle \varphi_{c(s)} \rangle = \begin{cases} \sqrt{\pi / 8 K_{c(s)}} & (M_{c(s)}^0 > 0) \\ 0 & (M_{c(s)}^0 < 0) \end{cases}. \tag{19}$$

Using the initial values of the coupling constants, given in (10–13), we obtain that flow trajectories in the charge sector (due to the SU(2)-charge symmetry) are along the separatrix $g_c = g_u$. Therefore, at

$$U + J_{xy} > 0, \tag{20}$$

there is a gap in the charge excitation spectrum ($\Delta_c \neq 0$) and the charge field $\varphi_c$ is ordered with the vacuum expectation value

$$\langle \varphi_c \rangle = 0, \tag{21}$$

while at $U + J_{xy} < 0$ the charge sector is gapless and the fixed-point value of the parameter $K_c^*$ is one.

The U(1) symmetry of the spin channel ensures more alternatives. Depending on the relation between the bare coupling constants there are two different strong-coupling sectors in the spin channel. For

$$U < \min\{0, J_{xy}\} \tag{22}$$

the spin channel is massive ($\Delta_s \neq 0$) and the field $\varphi_s$ gets ordered with the vacuum expectation value

$$\langle \varphi_s \rangle = 0, \tag{23}$$

while for

$$J_{xy} < \min\{0, U\} \tag{24}$$

the spin channel is massive ($\Delta_s \neq 0$), with vacuum expectation value

$$\langle \varphi_s \rangle = \sqrt{\frac{\pi}{8 K_s}}. \tag{25}$$

In all other cases the excitation spectrum in the corresponding channel is gapless. The low-energy behavior of the system is controlled by the fixed-point value of the Luttinger-liquid parameter $K_s^* = 1 + \frac{1}{2}g_s^*$. In the particular case of vanishing on-site interaction ($U = 0$) and antiferromagnetic exchange ($J_{xy} > 0$) one has to use a second order RG analysis to define accurately the fixed point value of the parameter $K_s$ (for details, see Ref. [25]).

## 2.1 Order parameters

To clarify the symmetry properties of the ground states of the system in different sectors we consider the following set of order parameters:

1) the on-site density operator $\rho(n) = \rho_\uparrow(n) + \rho_\downarrow(n)$

$$
: \hat{\rho}(n) := \sum_\alpha \left( c_{n,\alpha}^\dagger c_{n,\alpha} - 1 \right) \simeq \sqrt{\frac{2K_c}{\pi}} \partial_x \varphi_c
$$
$$
+ (-1)^n \sin\left( \sqrt{2\pi K_c} \varphi_c \right) \cos\left( \sqrt{2\pi K_s} \varphi_s \right), \quad (26)
$$

2) the on-site spin-density

$$
S_z(n) \simeq \sqrt{\frac{K_s}{2\pi}} \partial_x \varphi_s
$$
$$
+ (-1)^n \cos\left( \sqrt{2\pi K_c} \varphi_c \right) \sin\left( \sqrt{2\pi K_s} \varphi_s \right), (27)
$$

$$
S_x(n) \simeq \frac{i}{\pi a_0} \cos\left( \sqrt{2\pi K_s} \varphi_s \right) \sin\left( \sqrt{\frac{2\pi}{K_s}} \vartheta_s \right)
$$
$$
+ (-1)^n \cos\left( \sqrt{2\pi K_c} \varphi_c \right) \sin\left( \sqrt{\frac{2\pi}{K_s}} \vartheta_s \right), \quad (28)
$$

$$
S_y(n) \simeq \frac{-i}{\pi a_0} \cos\left( \sqrt{2\pi K_s} \varphi_s \right) \cos\left( \sqrt{\frac{2\pi}{K_s}} \vartheta_s \right)
$$
$$
+ (-1)^n \cos\left( \sqrt{2\pi K_c} \varphi_c \right) \sin\left( \sqrt{\frac{2\pi}{K_s}} \vartheta_s \right) \quad (29)
$$
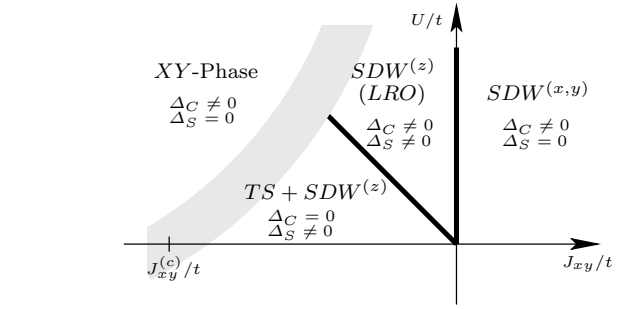
and in addition we use superconducting order parameters corresponding to

3a) the on-site singlet

$$
\mathcal{O}_S^\dagger(n) = c_{n,\uparrow}^\dagger c_{n,\downarrow}^\dagger
$$
$$
\sim \cos(\sqrt{2\pi K_s} \varphi_s) \exp\left( i\sqrt{\frac{2\pi}{K_c}} \vartheta_c \right)
$$
$$
- (-1)^n \sin(\sqrt{2\pi K_c} \varphi_c) \exp\left( i\sqrt{\frac{2\pi}{K_c}} \vartheta_c \right) (30)
$$

3b) the extended singlet

$$
\mathcal{O}_{ES}^\dagger(n) = \frac{1}{\sqrt{2}} \left( c_{n,\uparrow}^\dagger c_{n+1,\downarrow}^\dagger - c_{n,\downarrow}^\dagger c_{n+1,\uparrow}^\dagger \right)
$$
$$
\sim (-1)^n \cos\left( \sqrt{2\pi K_c} \varphi_c \right) \exp\left( i\sqrt{\frac{2\pi}{K_c}} \vartheta_c \right) (31)
$$



**Fig. 1.** The weak-coupling phase diagram of the itinerant $XY$-model at half-filling. Solid lines indicate borders between phases. The shaded region qualitatively marks the transition into the $XY$ magnetic phase ($J_{xy}^{(c)} \approx -4t$).

3c) and the triplet pairing

$$
\mathcal{O}_{TS^0}^\dagger(n) = \frac{1}{\sqrt{2}} \left( c_{n,\uparrow}^\dagger c_{n+1,\downarrow}^\dagger + c_{n,\downarrow}^\dagger c_{n+1,\uparrow}^\dagger \right)
$$
$$
\sim \sin\left( \sqrt{2\pi K_s} \varphi_s \right) \exp\left( i\sqrt{\frac{2\pi}{K_c}} \vartheta_c \right) \quad (32)
$$

$$
\mathcal{O}_{TS^\pm}^\dagger(n) = \frac{1}{\sqrt{2}} \left( c_{n,\uparrow}^\dagger c_{n+1,\uparrow}^\dagger \pm c_{n,\downarrow}^\dagger c_{n+1,\downarrow}^\dagger \right)
$$
$$
\sim \exp\left( i\sqrt{\frac{2\pi}{K_c}} \vartheta_c \right) \begin{cases} \cos\left( \sqrt{\frac{2\pi}{K_s}} \vartheta_s \right) \\ \sin\left( \sqrt{\frac{2\pi}{K_s}} \vartheta_s \right). \end{cases} \quad (33)
$$

Note that the smooth part in equation (30) corresponds to the usual BCS-type pairing while the oscillating terms in (30) and (31) describe the eta-pairing superconductivity [36].

## 2.2 Phases

With the results of the previous section for the excitation spectrum and the behavior of the corresponding fields equations (17–19) we now analyze the *weak-coupling* ground state phase diagram of the model (1) (see Fig. 1).

Let us first consider the case $U = 0$, where the weak-coupling analysis shows existence of two different phases: in the case of antiferromagnetic exchange, at $J_{xy} > 0$, there is a gap in the charge excitation spectrum while the spin sector is gapless. Ordering of the field $\varphi_c$ with vacuum expectation value $\langle \varphi_c \rangle = 0$ leads to a suppression of the CDW and *superconducting* correlations. The SDW and *Peierls* correlations show a power-law decay at large distances [25]. Due to the U(1)-spin symmetry, $K_s^* > 1$ and the *"in-plane"* correlations dominate in the ground state,

$$
\langle S^+(r) S^-(0) \rangle \sim r^{-K_s^* - 1/K_s^*} + (-1)^r r^{-1/K_s^*} \quad (34)
$$

while the longitudinal spin correlations

$$\langle S^z(r)S^z(0)\rangle \simeq r^{-2} + (-1)^r r^{-K_s^*} \qquad (35)$$

and *Peierls* correlations decay faster.

We now focus on the case of ferromagnetic exchange between spins. At $U = 0$ and $J_{xy} < 0$ there is a gap in the spin excitation spectrum while the charge excitation spectrum is gapless. As common in the half-filled band case, the gapless charge excitation spectrum opens a possibility for the realization of a *superconducting* instability in the system. Moreover, due to the U(1)-symmetry of the system, ordering of $\varphi_s$ with vacuum expectation value $\langle\varphi_s\rangle = \sqrt{\pi/8K_s}$ leads to a suppression of the CDW and singlet correlations as well as $S^z = \pm 1$ channels of the triplet pairing. However, the $S^z - S^z$ and triplet correlations in the $S^z = 0$ channel show an identical power-law decay

$$\langle S^z(r)S^z(0)\rangle = \langle \mathcal{O}_{TS}^\dagger(r)\mathcal{O}_{TS}(0)\rangle \simeq (-1)^r r^{-1} \quad (36)$$

at large distances and are the *dominating instabilities* in the system.

Let us now consider the effect of the on-site Coulomb repulsion. At $J_{xy} > 0$ the easy-plane antiferromagnetic phase remains unchanged at $U > 0$. However, at $J_{xy} < 0$ the TS+SDW$^{(z)}$ phase is stable only towards influence of a weak $U < -J_{xy}$ on-site coupling. In the case of repulsive Hubbard interaction, at $U > -J_{xy}$ a charge gap opens. This regime corresponds to the appearance of a long-range ordered *antiferromagnetic (Néel)* phase

$$\langle S^z(r)S^z(0)\rangle \sim \text{const.} \qquad (37)$$

in the ground state.

## 2.3 The ferromagnetic transition

Let us now discuss the ferromagnetic transition in the itinerant $XY$ model ($U = 0$). The very presence of this transition can already been seen within the weak-coupling studies, however detailed analysis of the phase diagram close to transition is out of scope of the continuum-limit approach. As we obtained, at $J_{xy} < 0$, $|J_{xy}| \ll t$, the charge excitation spectrum is gapless and the spin excitation spectrum is massive. However, in the limit of strong ferromagnetic exchange $|J_{xy}| \gg t$, the model is equivalent to the $XY$ spin chain. Therefore, with increasing coupling one has to expect a transition from the regime with massive spin and massless charge excitation spectrum into a insulating magnetic phase with gapless spin excitations. On the other hand, in the case of antiferromagnetic exchange $J_{xy} > 0$ the weak-coupling study shows a phase with gapless spin, gapped charge and dominating easy-plane spin correlations. One expects that this phase evolves smoothly to the strong coupling limit.

The $J_{xy} \leftrightarrow -J_{xy}$ asymmetry is already seen on the level of the Hartree regularization of the band-width cut-off parameter $W = 2\pi t$ as given by the equations (14)

$$W_{eff} = 2\pi \left(1 + \frac{J_{xy}}{2\pi t}\right). \qquad (38)$$

The weak-coupling approaches fail when the effective dimensionless coupling constant $|g_i| = \frac{J_{xy}}{2\pi t} = |g_i^c| \simeq 1$. This condition immediately gives $J_{xy}^{(c)} = -\pi t$. As we show below, using the DMRG studies of chains up to $L = 120$ sites, indeed the transition into the ferromagnetic easy-plane ordering discussed above takes place at $J_{xy}^{(c)} \sim -4t$.

# 3 Numerical results

We use the density-matrix renormalization-group (DMRG) method [37,38] to study the ground-state properties of this model. Our calculations have been performed for open chains up to 120 sites using the *infinite-size* version of the DMRG routine. A comparison with the *finite-size* algorithm, which requires more CPU time and memory, does not give a substantial improvement of the results. For most of the numerical results reported here we have kept 400 states in each block, which produces truncation errors smaller than $10^{-7}$.

In order to reduce edge effects we average correlation functions $C(|i - j|)$ over a number of pairs $(i, j)$ of lattice sites separated by the same displacement $r := |i - j|$ [39]. Typically we take nine pairs and for each value $r$ we place the pairs as close to the center of the chain as possible.

The asymptotic behavior of correlations (e.g. exponents) has been determined by an appropriate fitting of the data [40].

## 3.1 Excitation spectrum at U = 0

Let us start from the limiting case of the itinerant $XY$ model ($U = 0$) and analyze its excitation spectrum. The charge and spin gap for a half-filled $L$-site system are evaluated by

$$\Delta_C(L) = \frac{1}{2}\left[E_0\left(\frac{L}{2}+1, \frac{L}{2}+1\right) + E_0\left(\frac{L}{2}-1, \frac{L}{2}-1\right)\right.$$
$$\left. -2E_0\left(\frac{L}{2}, \frac{L}{2}\right)\right], \qquad (39)$$

$$\Delta_S(L) = E_0\left(\frac{L}{2}+1, \frac{L}{2}-1\right) - E_0\left(\frac{L}{2}, \frac{L}{2}\right), \qquad (40)$$

respectively, where $E_0(N_\uparrow, N_\downarrow)$ is the ground-state energy for $N_\uparrow$ up-spin and $N_\downarrow$ down-spin electrons. The extrapolation for $L \to \infty$ is then performed by fitting a polynomial in $1/L$ to the calculated finite-chain results. Figure 2 displays the extrapolated values as a function of $J_{xy}$.

We observe the following four sectors: at $J_{xy} > 0$ the system is characterized by gapless spin and gapped charge excitation spectrum, while the weak-coupling ferromagnetic sector exhibits gapless charge and gapful spin degrees of freedom.

Moreover, our numerical results show the presence of two new regions. At $J_{xy}^{(c1)} \approx -3t$ a charge gap opens, while the spin gap starts to decrease and finally closes at $J_{xy}^{(c2)} \approx -4t$. This defines two new sectors: for $J_{xy}^{(c2)} < J_{xy} < J_{xy}^{(c1)}$
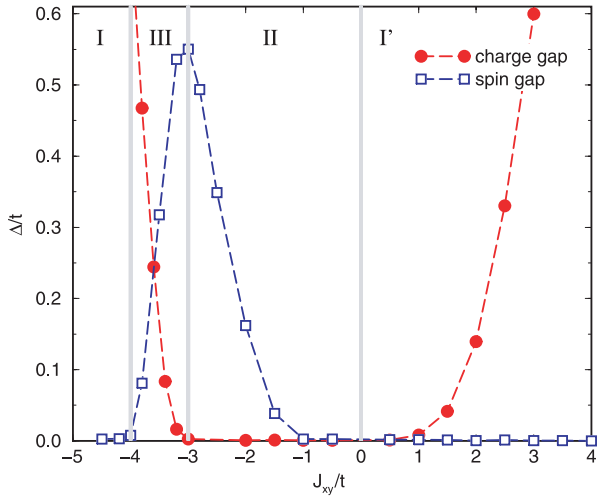
**Fig. 2.** Spin and charge excitation spectrum of the itinerant $XY$ model at half-filling. Depending on the behavior of the gaps four sectors can be distinguished. The approximate boundaries $J_{xy}^{(c1)} \approx -3t$ and $J_{xy}^{(c2)} \approx -4t$ are indicated by grey lines.

both the spin and charge sectors are gapped, while at $J_{xy} < J_{xy}^{(c2)}$ the spin sectors become gapless. There are no indications for further transitions in the system. Note that similar behavior of the gaps, with interchange of spin and charge degrees of freedom, was first observed by Sikkema and Affleck in the Penson-Kolb model [41].

## 3.2 Correlation functions at $U = 0$

To investigate the nature of ordering in the different phases we study the behavior of the correlation functions. In the sectors with gapless excitation spectrum and at half-filling we expect the usual expression for correlation functions

$$C(r) \equiv \langle \mathcal{O}^\dagger(r)\mathcal{O}(0)\rangle \sim A_1 r^{-\theta_1} + (-1)^r A_2 r^{-\theta_2} \quad (41)$$

consisting of a smooth part decaying with exponent $\theta_1$ and an oscillating part decaying with $\theta_2$. In determining the asymptotics of correlation functions we focus on the dominating part given by $\theta = \min\{\theta_1, \theta_2\}$.

In the following we will present results for correlation functions in different sectors of the phase diagram.

### 3.2.1 Sectors I and I' ($\Delta_C \neq 0$, $\Delta_S = 0$): The XY-phases

In Figure 3 we have plotted the longitudinal and transverse spin-spin correlations in the case of strong easy-plane exchange. Although the amplitudes of the transverse correlation functions are different, the estimated exponents are similar. In the case of ferromagnetic exchange we obtained $\theta \approx 0.57$, whereas for the antiferromagnetic exchange we have $\theta \approx 0.61$. The results are in a good agreement with the exact value $\theta = 0.5$ obtained for the $XY$-model [42]. The longitudinal correlation functions decay
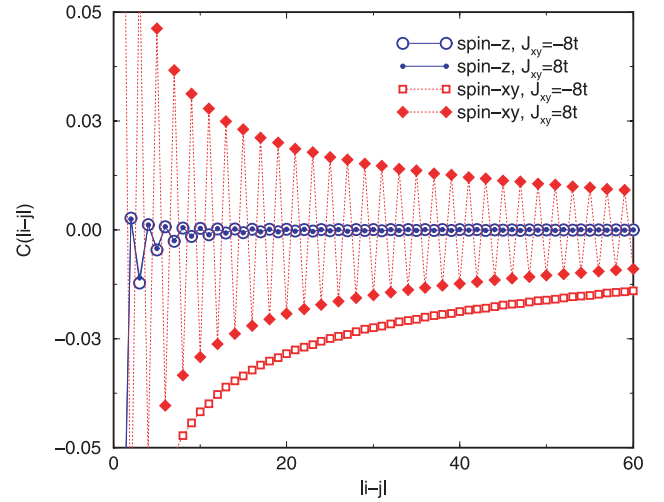


**Fig. 3.** The longitudinal (circle) and transverse (square and diamond) spin-spin correlations in the case of strong easy-plane ferromagnetic $J_{xy} = -8t$ (sector I) and antiferromagnetic $J_{xy} = 8t$ (sector I') exchange.
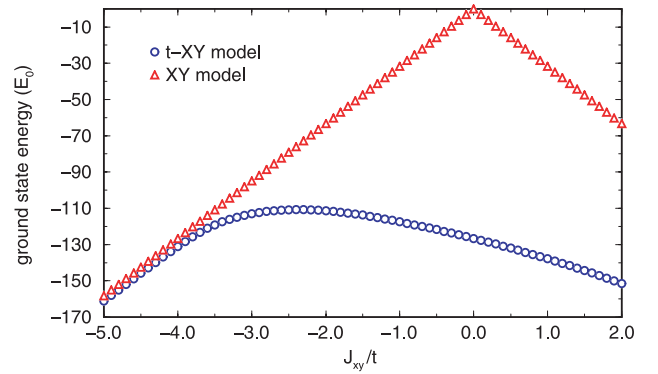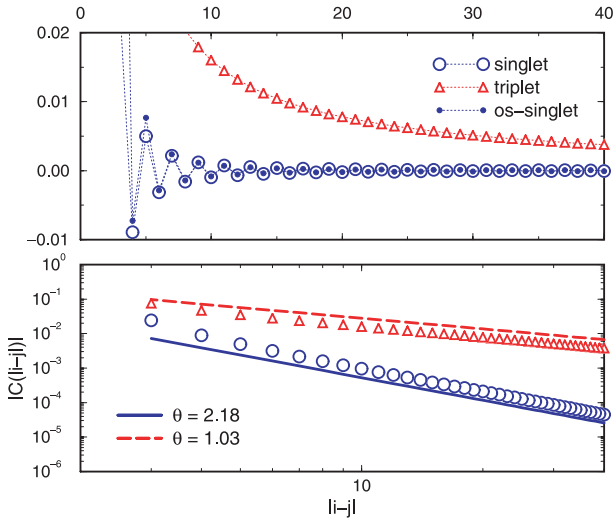


**Fig. 4.** Ground-state energy $E_0$ of the $XY$-model and the itinerant $XY$-model as a function of coupling $J_{xy}/t$ for a half-filled $L = 100$ chain.

faster. The calculated exponents $\theta \approx 1.79$ (for $J_{xy} = -8t$) and $\theta \approx 1.66$ (for $J_{xy} = 8t$) are close to the exact $XY$-value $\theta = 2$.
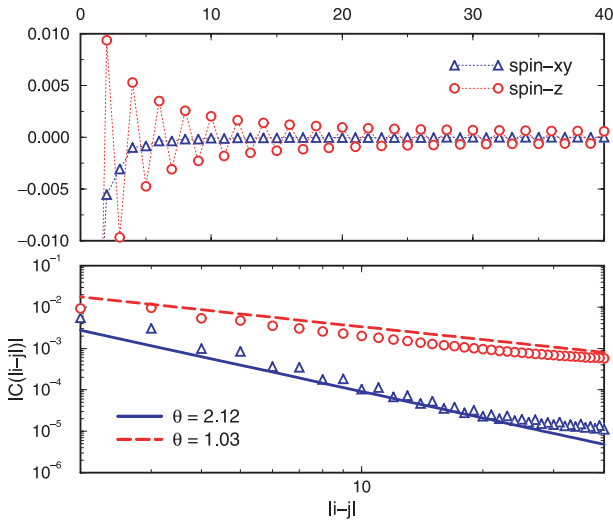
The asymmetry of this model is clearly seen in Figure 4, where the ground state energy as a function of $J_{xy}$ is presented. As we observe from Figure 4 in the case of ferromagnetic exchange the ground state energy of the itinerant model becomes very close to that of the spin-$\frac{1}{2}$ $XY$ chain.

### 3.2.2 Sector II ($\Delta_C = 0$, $\Delta_S \neq 0$): The TS+SDW$^{(z)}$ regime

Let us now focus on the case of ferromagnetic exchange $J_{xy} < 0$ at $U = 0$. The bosonization results predict a suppression of the CDW and singlet correlations, whereas SDW$^{(z)}$ and triplet correlators show identical power-law decay (cf. with Eq. (36)). Furthermore, they are the dominating instabilities in this phase. Figure 5 displays DMRG results for the singlet- and triplet-pair correlation function. One can clearly observe a strong triplet-pair
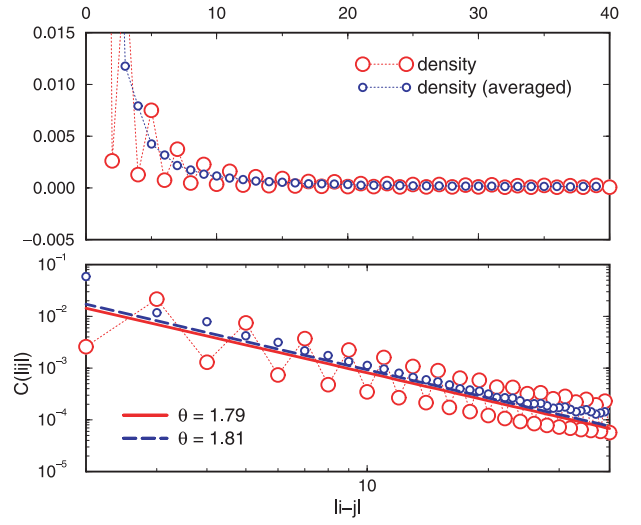
**Fig. 5.** Pair correlation functions in the case of ferromagnetic exchange $J_{xy} = -2t$ and $U = 0$ (sector II). The lower figure shows the algebraic decay of the triplet and singlet correlation, plotted on a double logarithmic scale.



**Fig. 7.** DMRG results for the density-density correlation function at $J_{xy} = -2t$ (sector II) including the average value of this correlation which removes the even-odd-$r$ oscillations.

change ($J_{xy} = -2t$). We observe that the correlation functions exhibit an algebraic decay in which the transverse spin-spin correlation function decays faster. The calculated exponent of the longitudinal spin correlation function is, in agreement with bosonization results, close to that of the triplet-pairing correlations. Compared to the other results, the scaling behavior of the spin correlations is not very good in this sector. However, we have verified that with increasing system size and number of states kept in the DMRG algorithm the region with algebraic decay increases. Nevertheless, the numerical estimates for the exponents are less reliable than those for other correlation functions.

To complete the weak-coupling picture of sector II, we performed calculations for the density-density correlation. The results are shown in Figure 7. Since in the double logarithmic plot we observe strong oscillations we additionally calculate the average value [43]

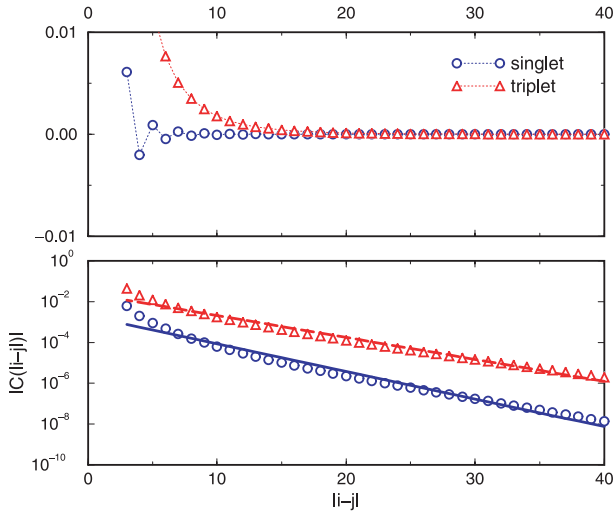$$\bar{C}(r) = \frac{1}{4}[C(r-1) + 2C(r) + C(r+1)] \qquad (42)$$

to smoothen the curve. As its clearly seen from the lower part of Figure 7 the oscillations are removed, but the estimated exponent remains almost unchanged. Thus the DMRG result indicates a fast decay of density-density correlations, in agreement with the bosonization results.

Therefore, we can conclude that coexisting triplet-pairing and antiferromagnetic SDW$^{(z)}$ ordering are the dominating instabilities in this sector.

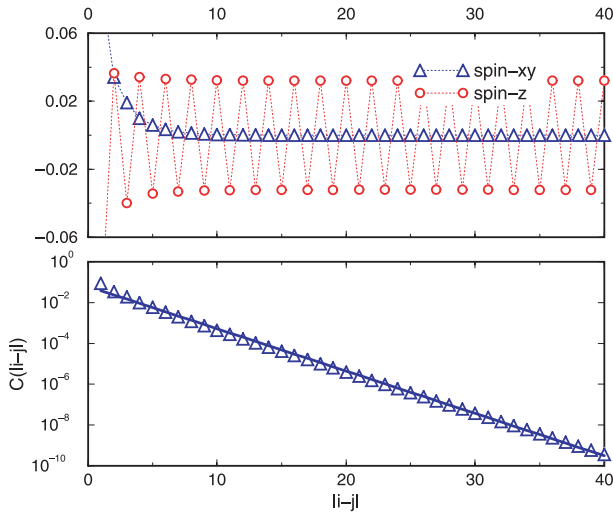### 3.2.3 Sector III ($\Delta_C \neq 0$, $\Delta_S \neq 0$): The intermediate phase

In this subsection we analyze the intermediate sector at $-4t \leq J_{xy} \leq -3t$ which is absent in the weak-coupling phase diagram (cf. with Fig. 1).

We start to examine the asymptotic behavior of the superconducting and spin-spin correlations. In Figure 8



**Fig. 6.** DMRG results for the longitudinal and transversal spin correlation function, plotted against the real space distance $|i - j|$ (upper figure) at $J_{xy} = -2t$ (sector II). The exponents (lower figure) were calculated using a suitable subset of the data to reduce finite size effects and numerical inaccuracies at large distances.

correlation. Note that the on-site and extended singlet-pair correlations show an almost identical behavior. This is expected from the bosonization results (30) and (31) since the smooth part of the on-site singlet correlations (30) does not contribute due to (25). In the double logarithmic plot (see lower figure) all correlation functions indicate a power-law decay with fast decaying singlet-pairing correlators ($\theta \approx 2.18$) and a slowly decaying triplet correlation function ($\theta \approx 1.03$). The results are in a good agreement with those predicted by bosonization.

In Figure 6 we show calculations for the longitudinal and transversal spin-spin correlation for ferromagnetic ex-

**Fig. 8.** Pair correlation functions at $J_{xy} = -3.5t$ and $U = 0$ (sector III). The lower part shows a double logarithmic plot with linear fits.
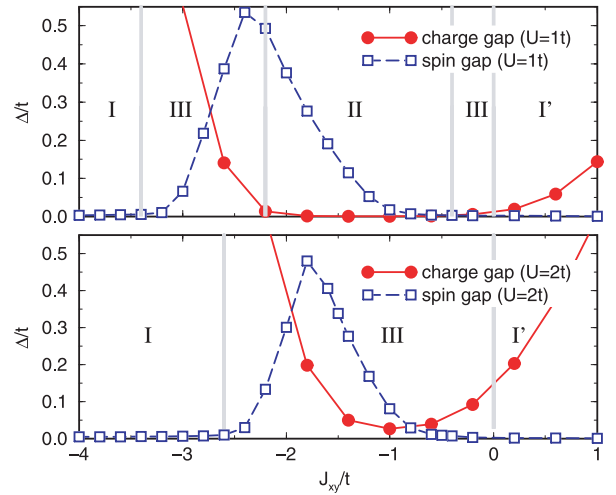


**Fig. 9.** Spin correlation functions at $J_{xy} = -3.5t$ and $U = 0$ (sector III). The lower part shows a double logarithmic plot with a linear fit.



**Fig. 10.** Spin and charge excitation gaps of the itinerant $XY$ model at $U = t$ (upper figure) and $U = 2t$ (lower figure).

### 3.3 Behavior for nonvanishing on-site interaction

#### 3.3.1 Excitation spectrum at U $\neq$ 0

Let us now consider the effects of a repulsive Coulomb interaction on the ground state phase diagram of the model. We start with the excitation spectrum.
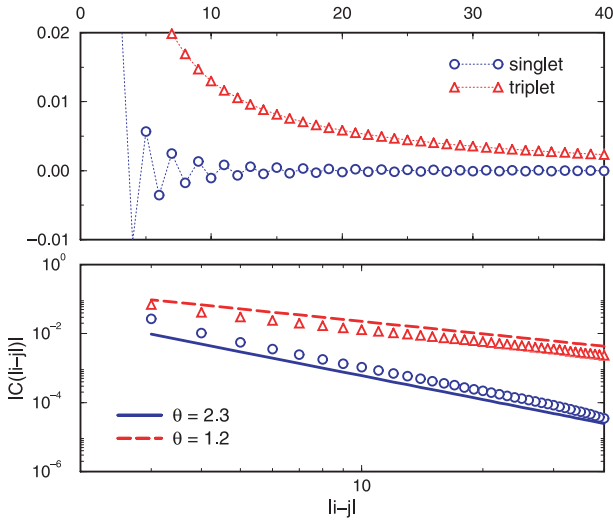
From the bosonization results we know the general effect of the Coulomb repulsion on the phase diagram which displays itself in an enlargement of the charge gap sectors at the expense of the spin gap sector. Figure 10 shows charge and spin gaps for $U = t$ and $U = 2t$. One can clearly see that sectors I and I', where we have a finite charge gap $\Delta_C > 0$, are enlarged. As a consequence the spin-gapped phase (sector II) becomes smaller with increasing $U$ and finally vanishes completely. Already at $U = 2t$ the charge gap is always finite. Thus the main effect of the presence of Coulomb interactions is the suppression of sector II, i.e. a reduction of the region with dominating superconducting correlations. In analogy with the $U = 0$ case we conclude that the sectors with magnetic correlations become dominating.
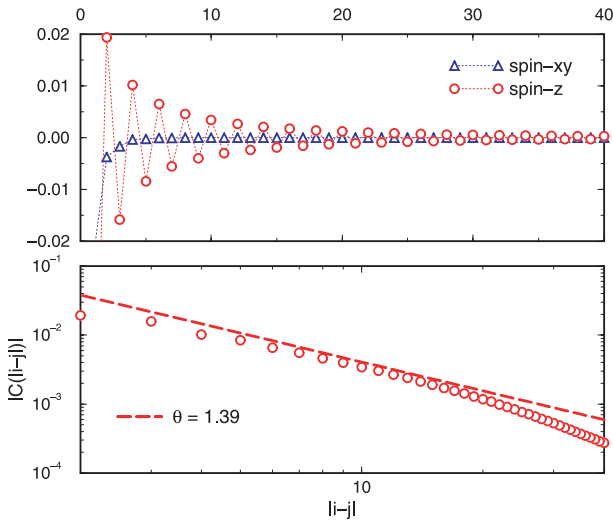
#### 3.3.2 Correlation functions at U $\neq$ 0

In the following we analyze the effect of the Coulomb interactions on pair and spin correlation functions. We will focus on the behavior in sectors II and III where $\Delta_C = 0$, $\Delta_S \neq 0$ and $\Delta_C \neq 0$, $\Delta_S \neq 0$, respectively.

In the TS + SDW$^{(z)}$ phase we consider the coupling $J_{xy} = -1.5t$ at $U = t$ as a representative point. The phase is characterized by a spin gap of magnitude $\Delta_S \approx 0.13t$ and massless charge mode. The asymptotic behavior of the pair and spin correlation functions is plotted in Figure 11 and Figure 12, respectively. One can clearly see that the triplet-pairing and longitudinal spin-spin correlations represent the dominating instabilities in the system. Unfortunately the accuracy of the numerics is not sufficient in this case to verify that the exponents are still

we present DMRG data for the pairing correlation functions. As is clearly seen from the figure, especially from the logarithmic plot, the superconducting correlations decay exponentially in agreement with the presence of a charge gap.

In Figure 9 we plot the spin-spin correlation functions. The logarithmic plot shows that the transverse spin correlation functions decay exponentially. Contrary, the longitudinal spin correlations show well-established long-range order.

The appearance of LRO is consistent with the U(1)⊗Z$_2$ spin-symmetry of the present model (1). The continuous U(1) symmetry is generated by the operators $S^x$ and $S^y$, while the discrete Z$_2$ symmetry comes from the invariance with respect to the $S^z \rightarrow -S^z$ transformation. Since the SDW$^z$ ordering violates the discrete Z$_2$ and translation symmetries, the true LRO state is not forbidden.

**Fig. 11.** Pair correlation functions in the ferromagnetic phase at $J_{xy} = -1.5t$ and $U = t$ (sector II). The lower figure shows the algebraic decay of the triplet and singlet correlation, plotted on a double logarithmic scale.
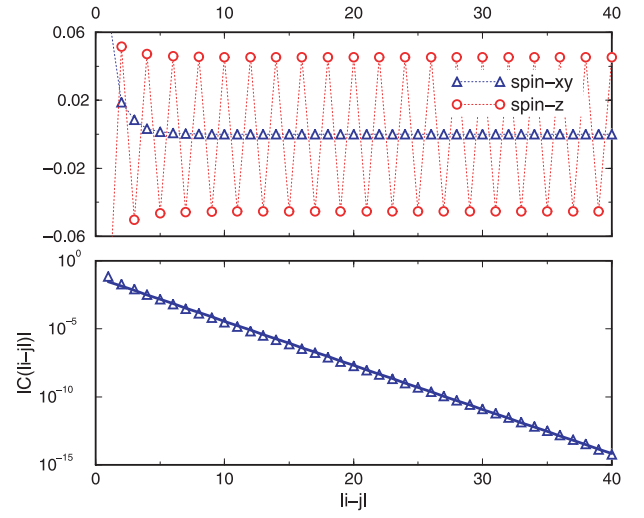


**Fig. 12.** Spin correlation functions at $J_{xy} = -1.5t$ and $U = t$ (sector II). Lower figure is plotted on a double logarithmic scale showing an algebraic decay for the longitudinal correlator and exponentially decaying behavior for the transversal correlation function.



**Fig. 13.** Spin correlation functions at $J_{xy} = -2t$ and $U = 2t$ (sector III). Upper figure indicates LRO fluctuation for the longitudinal spin correlation function.



**Fig. 14.** Spin correlation functions at $J_{xy} = -4t$ and $U = 2t$ (sector I).

exactly identical. Instead, we find $\theta \approx 1.2$ (triplet pairing) and $\theta \approx 1.39$ (longitudinal spin).
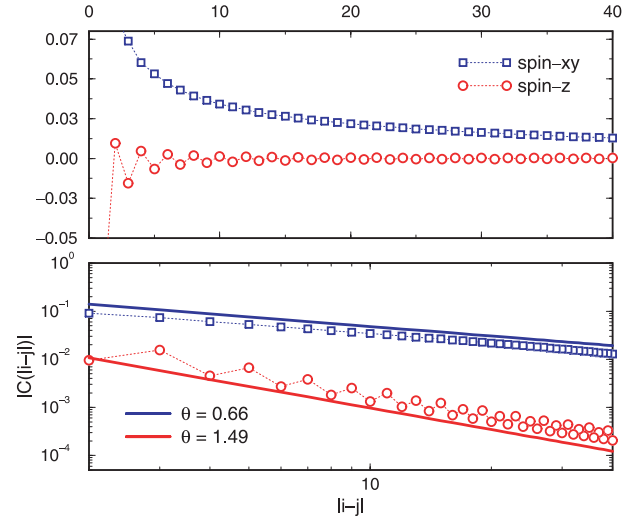
In the SDW$^{(z)}$ phase with LRO we compute the correlation functions at $U = 2t$ and $J_{xy} = -2t$. The presence of a charge gap $\Delta_C \approx 0.38t$ leads now to an exponential decay of superconducting correlations.

On the other hand, as is clearly seen from Figure 13, the longitudinal spin-spin correlations show a true LRO while the transverse spin correlations decay exponentially.

In ferromagnetic phase we use as a representative point $U = 2t$ and $J_{xy} = -4t$. As one can observe from Figure 14 the longitudinal spin-spin correlations are exponentially suppressed, while the decay of the transverse ferromag-

netic spin correlations is almost identical to that of the standard $XY$-chain.

## 4 Conclusions

Motivated by recent experimental findings that show evidence for the competition or even coexistence of superconductivity and magnetism we have investigated the ground state properties of an itinerant $XY$ model.

First we considered the case of vanishing on-site Coulomb interactions. The behavior of spin and charge gaps as function of the spin-coupling $J_{xy}$ allows to distinguish four different phases (cf. with Fig. 15). For antiferromagnetic interactions $J_{xy} > 0$ the spin gap vanishes, but the charge gap is always finite. The observed behavior of the correlation functions indicates a smooth evolution to
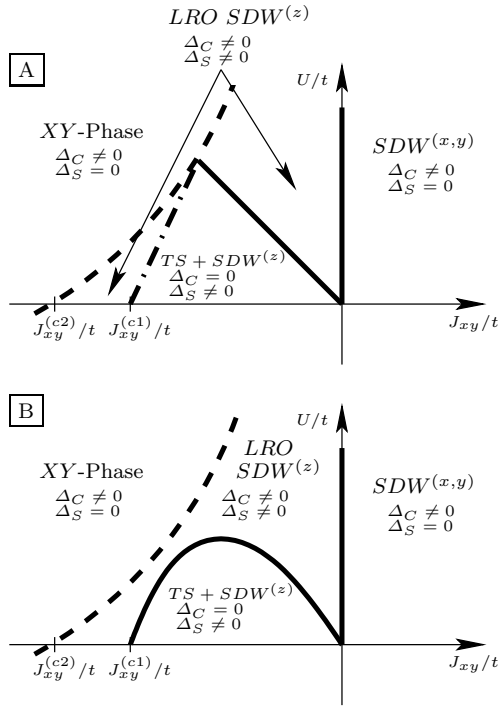
**Fig. 15.** The possible ground state phase diagram of the itinerant $XY$-model at half-filling. Solid lines mark second order phase transitions between the phases as obtained from bosonization. The dashed line corresponds to the spin-flop transition from the LRO SDW$^{(z)}$ into the ferromagnetic $XY$ phase ($J_{xy}^{(c2)} \approx -4t$). The dashed-dotted line marks the metal-insulator transition from the spin-gapped metallic phase with identical decay of triplet superconducting and SDW$^{(z)}$ correlations into the LRO antiferromagnetic (SDW$^{(z)}$) phase ($J_{xy}^{(c1)} \approx -3t$). Our numerical results do not exclude the possibility that the multicritical point given in $\boxed{A}$ is an artifact of the bosonization approach. In a more realistic scenario of the phase diagram the SDW$^{(z)}$ always separates the superconducting phase from the easy-plane ferromagnetic phase as it is shown $\boxed{B}$.

the limiting case of spin-1/2 antiferromagnetic $XY$ chain at $J_{xy} \to \infty$.

For ferromagnetic couplings $J_{xy} < 0$ three different phases appear. Already for weak interactions a spin gap opens, but the charge sector is gapless. Here SDW$^{(z)}$ and triplet correlations, which decay with similar power-laws, are dominating, i.e. this regime exhibits a coexistence of antiferromagnetic ordering and triplet superconductivity. At $J_{xy}^{(c1)} \approx -3t$ the spin gap is maximal and a charge gap opens. This intermediate phase, that extends up to $J_{xy}^{(c2)} \approx -4t$, shows long-range order in the longitudinal spin correlation, whereas superconducting correlations are suppressed and decay exponentially as expected for the case of a finite charge gap. Finally, at $J_{xy} > -4t$ via a spin-flop transition the system again enters a $XY$ phase characterized by vanishing spin but finite charge gap. Here the behavior is similar to the ferromagnetic $XY$ model.

The presence of a repulsive on-site Coulomb interaction $U$ has a strong effect on the phase diagram. Generically it leads to an enlargement of the sectors with non-vanishing charge gap at the expense of the sectors with spin gap. Already at $U = 2t$ the charge gap is finite for all values of the exchange coupling $J_{xy}$. Therefore the phase where antiferromagnetism and triplet superconductivity coexist is no longer observed and magnetic correlations become dominant everywhere. Only for small values of the Coulomb interaction there is still a finite window of coexistence possible.

Figure 15 summarizes our findings. The phase diagram shown combines results from bosonization (cf. Fig. 1) and DMRG. However, it is difficult to determine the location of the phase boundaries numerically. E.g. it still has to be clarified whether the coexistence phase extends up to the $XY$-phase such that two LRO SDW$^{(z)}$ phases exist (Fig. 15a). Alternatively, only one LRO SDW$^{(z)}$ phase exists such that it always separates the superconducting from the ferromagnetic $XY$-phase (Fig. 15b).

## References

1. A.V. Chubukov, D. Pines, J. Schmalian, in *The Physics Superconductors*, edited by K.H. Bennemann, J.B. Ketterson (Springer-Verlag 2003), p. 495
2. For a review, see A.P. Mackenzie, Y. Maeno, Rev. Mod. Phys. **75**, 657 (2003)
3. S.S. Saxena, P. Agarwal, K. Ahilan, F.M. Grosche, R.K.W. Haselwimmer, M.J. Steiner, E. Pugh, I.R. Walker, S.R. Julian, P. Monthoux, G.G. Lonzarich, A. Huxley, I. Sheikin, D. Braithwaite, J. Flouquet, Nature **406**, 587 (2000)
4. D. Aoki, A. Huxley, E. Ressouche, D. Braithwaite, J. Flouquet, J.-P. Brison, E. Lhotel, C. Paulsen, Nature **413**, 613 (2001)
5. C. Pfleiderer, M. Uhlarz, S.M. Hayden, R. Vollmer, H.v. Löhneysen, N.R. Bernhoeft, G.G. Lonzarich, Nature **412**, 58 (2001)
6. T.M. Rice, M. Sigrist, J. Phys.: Condens. Matter **7**, L643 (1995)
7. I.I. Mazin, D.J. Singh, Phys. Rev. Lett. **79**, 733 (1997)
8. M. Sigrist, D. Agterberg, A. Furusaki, C. Honercampf, K.K. Ng, T.M. Rice, M.E. Zhitomirsky, Physica C **318**, 134 (1999)
9. T.R. Kirkpatrick, D. Belitz, T. Vojta, R. Narayanan, Phys. Rev. Lett. **87**, 127003 (2001)
10. D.J. Singh, I.I. Mazin, Phys. Rev. Lett. **88**, 187004 (2002)
11. M.B. Walker, K.V. Samokhin, Phys. Rev. Lett. **88**, 227001 (2002)
12. A.V. Chubukov, A.M. Finkel'stein, R. Haslinger, D.K. Morr, Phys. Rev. Lett. **90**, 077002 (2003)

13. A.I. Buzdin, A.S. Mel'nikov, Phys. Rev. B **67**, 020503 (2003)
14. T.R. Kirkpatrick, D. Belitz, Phys. Rev. B **67**, 024515 (2003)
15. D. Jérome, A. Mazaud, M. Ribault, K. Bechgaard, J. Phys. France Lett. **41**, L92 (1980)
16. T. Ishiguro, K. Tamaji, G. Saito, *Organic Superconductors* 2nd edn. (Springer 1998)
17. M. Takigawa, H. Yosuoka, G. Saito, J. Phys. Soc. Jpn **56**, 873 (1987); I.J. Lee, M.J. Naughton, G.M. Danner, P.M. Chaikin, Phys. Rev. Lett. **78**, 3555 (1997); S. Belin, K. Behnia, Phys. Rev. Lett. **79**, 2125 (1997); I.J. Lee, S.E. Brown, W.G. Klark, M.J. Strouse, M.J. Naughton, W. Kang, P.M. Chaikin, Phys. Rev. Lett. **88**, 017004 (2002); I.J. Lee, D.S. Show, W.G. Klark, M.J. Strouse, M.J. Naughton, P.M. Chaikin, S.E. Brown, Phys. Rev. B **68**, 092510 (2003)
18. D. Jérome, Science **252**, 1509 (1991)
19. T. Vuletic, P. Auban-Senzier, C. Pasquier, S. Tomic, D. Jérome, M. Héritier, K. Bechgaard, Eur. Phys. J. B **25**, 319 (2002)
20. A.V. Kornilov, V.M. Pudalov, Y. Kitaoka, K. Ishida, G.-Q. Zheng, T. Mito, J.S. Qualls, `cond-mat/0307021`
21. S. Lefebvre, P. Wzietek, S. Brown, C. Bourbonnais, D. Jérome, C. Mézière, M. Fourmigué, P. Batail, Phys. Rev. Lett. **85**, 5420 (2000)
22. For a review, see E. Dagotto, Rev. Mod. Phys. **66**, 763 (1994)
23. A. Mielke, J. Phys. A **24**, L73 (1991); A. Mielke, H. Tasaki, Comm. Math. Phys. **158**, 341 (1993); H. Tasaki, Phys. Rev. Lett. **69**, 1608 (1992); H. Tasaki, Phys. Rev. Lett. **75**, 4678 (1995); E. Müller-Hartmann, J. Low. Temp. Phys. **99**, 349 (1995)
24. H. Mukuda, K. Ishida, Y. Kitaoka, K. Asayama, Z.Q. Mao, Y. Mori, Y. Maeno, Physica B **259-261**, 944 (1999)
25. G.I. Japaridze, E. Müller-Hartmann, Phys. Rev. B **61**, 9019 (2000)
26. K.A. Penson, M. Kolb, Phys. Rev. B **33**, 1663 (1986)
27. G.I. Japaridze, A.P. Kampf, M. Sekania, P. Kakashvili, Ph. Brune, Phys. Rev. B **65**, 014518 (2002)
28. J. Sólyom, Adv. Phys. **28**, 201 (1979)
29. Y. Hasegava, H. Fukuyama, J. Phys. Soc. Jpn **55**, 3978 (1986); J. Phys. Soc. Jpn **56**, 877 (1987)
30. V.J. Emery, in *Highly Conducting One-Dimensional Solids*, edited by J.T. Devreese, R.P. Evrard, V.E. Van Doren (Plenum, New York, 1979)
31. J. Voit, Phys. Rev. B **45**, 4027 (1992)
32. For a recent review, see A.O. Gogolin, A.A. Nersesyan, A.M. Tsvelik, *Bosonization and strongly correlated systems* (Cambridge University Press, 1998)
33. J.M. Kosterlitz, D.J. Thouless, J. Phys. C **11**, 1583 (1973)
34. P. Wiegmann, J. Phys. C **11**, 1583 (1978)
35. K.A. Muttalib, V.J. Emery, Phys. Rev. Lett. **57**, 1370 (1986); T. Giamarchi, H.J. Schulz, J. Phys. France **49**, 819 (1988); T. Giamarchi, H.J. Schulz, Phys. Rev. B **33**, 2066 (1988)
36. C.N. Yang, Phys. Rev. Lett. **63**, 2144 (1989)
37. S.R. White, Phys. Rev. Lett. **69**, 2863 (1992); S.R. White, Phys. Rev. B **48**, 10345 (1993)
38. *Density-Matrix Renormalization*, edited by I. Peschel, X. Wang, M. Kaulke, K. Hallberg (Springer, 1999)
39. R.M. Noack, S.R. White, D.J. Scalapino, Phys. Rev. Lett. **73**, 882 (1994)
40. C. Dziurzik, dissertation, Universität zu Köln (2003)
41. A. Sikkema, I. Affleck, Phys. Rev. B **52**, 10207 (1995)
42. E. Lieb, T. Schultz, D. Mattis, Ann. Phys. (NY) **16**, 407 (1961)
43. K.A. Hallberg, P. Horsch, G. Martinez, Phys. Rev. B **52**, R719 (1995)